# Supplemental Material for "Critical properties of the two-dimensional $q$-state clock model"

Zi-Qian Li,[1,2] Li-Ping Yang,[3] Z. Y. Xie,[4] Hong-Hao Tu,[5,*] Hai-Jun Liao,[1,6,†] and T. Xiang[1,2,7,‡]

[1]*Institute of Physics, Chinese Academy of Sciences, Beijing 100190, China*
[2]*University of Chinese Academy of Sciences, Beijing 100049, China*
[3]*Department of Physics, Chongqing University, Chongqing 401331, China*
[4]*Department of Physics, Renmin University of China, Beijing 100872, China*
[5]*Institute of Theoretical Physics, Technische Universität Dresden, 01062 Dresden, Germany*
[6]*Songshan Lake Materials Laboratory, Dongguan, Guangdong 523808, China*
[7]*Collaborative Innovation Center of Quantum Matter, Beijing 100190, China*

This supplemental material provides more detailed descriptions of the tensor network representation of the $q$-state clock model and its dual model, VUMPS algorithm and results, derivation of the boson radius for $q \geq 5$, $\mathbb{Z}_q$ deformed sine-Gordon theory, and Klein bottle entropy approach.

### A. Tensor network representation of the $q$-state clock model and its dual model

The ferromagnetic $q$-state clock model on the 2D square lattice is defined by the Hamiltonian

$$H = -J \sum_{\langle ij \rangle} \cos(\theta_i - \theta_j), \tag{S1}$$

where $\langle ij \rangle$ refers to the nearest neighbors, $\theta_i = 2\pi k/q$ denotes a discrete angle variable with $k = 0, 1, \ldots, q-1$ at site $i$, and $J = 1$ sets the energy scale.

To derive the tensor network representation of the partition function, we use the character expansion of the local Boltzmann weight

$$e^{\beta \cos(\theta_i - \theta_j)} = \sum_{m=0}^{q-1} V_{\theta_i, m} \lambda_m V^*_{\theta_j, m}, \tag{S2}$$

where $V_{\theta_i, m} = e^{im\theta_i}/\sqrt{q}$ is a unitary matrix, and $\lambda_m$ is a diagonal matrix (bond spectrum) defined by

$$\lambda_m = \sum_{\theta} e^{-im\theta} e^{\beta \cos(\theta)}/\sqrt{q} = \sum_{\theta} \cos(m\theta) e^{\beta \cos(\theta)}/\sqrt{q}. \tag{S3}$$

Then, the partition function $Z = \sum_{\{\theta_i\}} e^{-\beta H}$ can be cast into the following tensor network representation:

$Z = \mathrm{Tr}$ 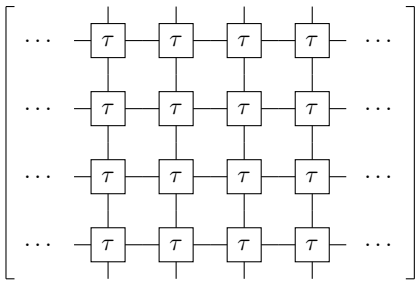 (S4)

where the local tensor $\tau_{ijkl}$ [see Fig. 1(a)] at each site is given by [S1]

$$\tau_{ijkl} = \sqrt{\lambda_i \lambda_j \lambda_k \lambda_l}\, \delta_{\mathrm{mod}(i+j-k-l,q),0}. \tag{S5}$$

Furthermore, the dual spin variables can be defined with a Kramer-Wannier dual transformation [S2] as follows [see Fig. 1(b)]:

$$\sigma_1 = \theta_1 - \theta_4, \qquad \sigma_2 = \theta_2 - \theta_1, \qquad \sigma_3 = \theta_2 - \theta_3, \qquad \sigma_4 = \theta_3 - \theta_4. \tag{S6}$$

Thus, the partition function of the dual model can also be represented as a tensor network, defined by another local tensor

$$\tau_{\sigma_1 \sigma_2 \sigma_3 \sigma_4} = \sqrt{\Lambda_{\sigma_1} \Lambda_{\sigma_2} \Lambda_{\sigma_3} \Lambda_{\sigma_4}}\, \delta_{\mathrm{mod}(\sigma_1 + \sigma_2 - \sigma_3 - \sigma_4, q), 0}, \tag{S7}$$

where $\Lambda_\sigma = \sqrt{q}e^{\beta\cos\sigma}$.

One advantage of the tensor network representation is that the self-dual points for $q = 2, 3, 4, 5$ become manifest

$$\beta_{\rm sd} = \begin{cases} \frac{1}{2}\ln(\sqrt{2}+1), & q=2 \\ \frac{2}{3}\ln(\sqrt{3}+1), & q=3 \\ \ln(\sqrt{2}+1), & q=4 \end{cases} \tag{S8}$$

and

$$\frac{e^{5\beta_{\rm sd}/4}}{\cosh\left(\sqrt{5}\beta_{\rm sd}/4\right)} = \sqrt{5}+1, \qquad q=5. \tag{S9}$$

For $q = 5$, the numerical solution to Eq. (S9) gives $\beta_{\rm sd} \approx 1.0763180716046478$ ($T_{\rm sd} \approx 0.929093384550472$) [S1].

### B. VUMPS algorithm and results

This section provides a brief review of the VUMPS algorithm [S3]. We emphasize on how to use it to calculate the physical quantities, such as the free energy, magnetization, internal energy, entanglement entropy, and correlation length.

The VUMPS method works in the thermodynamic limit and determines the fixed-point MPS, which approximates the leading eigenvector corresponding to the largest eigenvalue of the row-to-row transfer matrix, namely,

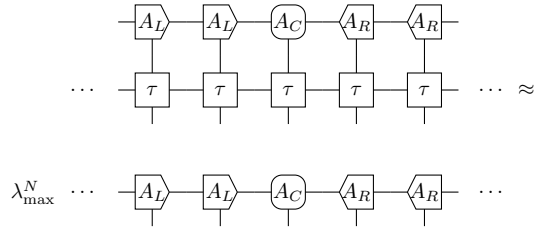


(S10)

where $\lambda_{\rm max}$ is the largest eigenvalue per site of the row-to-row transfer matrix, which is related to free energy density per site by $f = -k_B T \ln(\lambda_{\rm max})$. Furthermore, the fixed-point MPS satisfies the mixed canonical form conditions

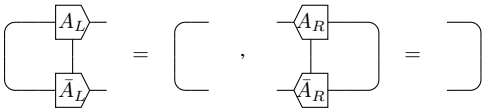


(S11)

and $A_L$, $A_R$, and $A_C$ near or at the fixed-point satisfy

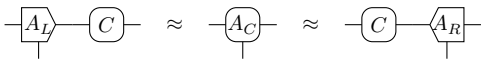


(S12)

To determine the fixed-point tensors $A_L$, $A_R$, and $A_C$, the VUMPS algorithm includes the following four steps:

1. Find the left and right environments $E_L$ and $E_R$ by power or Arnoldi method:

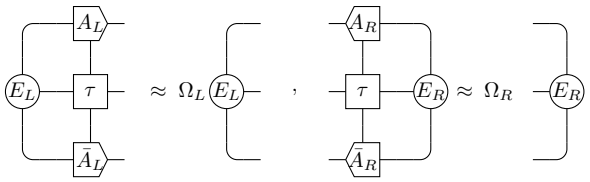


(S13)

2. Find the central tensors $C$ and $A_C$ by power or Arnoldi method:

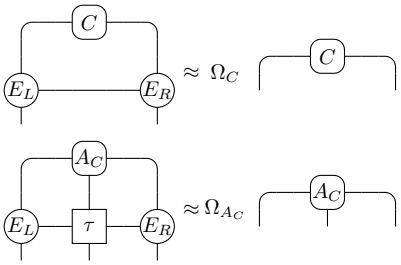


(S14)

where $\Omega_{A_C}/\Omega_C \approx \Omega_L \approx \Omega_R$ is approximately equal to the largest eigenvalue $\lambda_{\max}$ of the row-to-row transfer matrix near or at the fixed point.

3. Obtain new $A_L$ and $A_R$ from $A_C$ and $C$ using polar decompositions or QR decompositions [S3] (here we use QR decompositions)

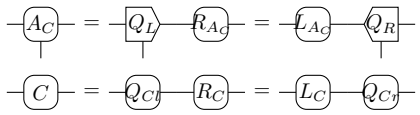


(S15)

where $Q_L, Q_R, Q_{Cl}$ and $Q_{Cr}$ are unitary matrices, and the diagonal entries of $R_{A_C}, L_{A_C}, R_C$ and $L_C$ are positive. Then, we obtain

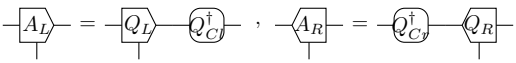


(S16)

4. Repeat the steps 1-3, until the error of the fixed point [Eq. (S12)] is less than a certain threshold.

Once the fixed-point MPS is obtained, various physical quantities can be calculated. The entanglement spectrum of the fixed-point MPS corresponds to the squared singular values $s_n$ of the tensor $C$ [see Eq. (S12)]. Thus, the entanglement entropy $S_{\rm E}$ of the fixed-point MPS can be readily calculated as follows:

$$S_{\rm E} = -\sum_{n=1}^{D} s_n^2 \ln s_n^2, \tag{S17}$$

where $D$ is the bond dimension of the fixed-point MPS, and $\sum_{n=1}^{D} s_n^2 = 1$.

The correlation length can be calculated by

$$\xi \equiv -1/\ln|\epsilon_2/\epsilon_1|, \tag{S18}$$

where $\epsilon_1$ and $\epsilon_2$ are the largest and the second largest eigenvalues of the transfer matrix

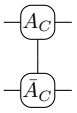


(S19)

respectively.

The expectation value of a local physical quantity $X$, such as magnetization, can be calculated by means of an impurity tensor $\tau_X$

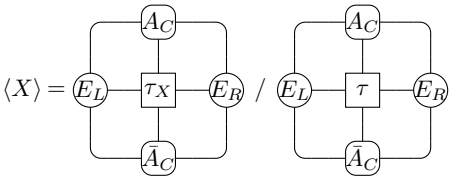


(S20)

For example, the impurity tensor of the magnetization $M \equiv \langle e^{i\theta} \rangle$ is defined as

$$\tau_M(i,j,k,l) = \sqrt{\lambda_i \lambda_j \lambda_k \lambda_l}\, \delta_{\mathrm{mod}(i+j-k-l+1,q),0}. \tag{S21}$$

The local physical quantities of the dual model can be calculated in a similar fashion.

Fig. S1 shows the magnetization $M$, the entanglement entropy $S_{\rm E}$ of the fixed-point MPS, and the correlation length $\xi$ for $q = 5, 6, 7$ and 8 clock models (red curves) and their corresponding dual models (blue curves). It is observed in Fig. S2 that the above physical quantities of the clock model at the rescaled temperature $T/T_{\rm sd}$ well coincide with those of the dual model at the rescaled inverse temperature $T_{\rm sd}/T$, especially for $q = 5$ case, whose exact self-dual point $T_{\rm sd} \approx 0.929093384550472$ is known. This agreement gives a strong hint on the possible existence of the self-duality.

The first row of Fig. S3 shows the central charge $c$ extracted by linearly fitting the slope between $S_{\rm E}$ and $\ln(\xi)/6$ at representative point $T = 0.928, 0.794, 0.693$ and $0.614$ in the critical phase for the clock model with $q = 5, 6, 7$ and 8, respectively. The second row of Fig. S3 shows the critical temperatures $T_{c1}$ and $T_{c2}$ extracted by linearly extrapolating the peak positions $T_1^*(D)$ and $T_2^*(D)$ of $S_{\rm E}$ with $(\ln \xi^*(D))^{-2}$, where $\xi^*(D)$ is the correlation length at the peak position for a given bond dimension $D$. Table S1 summarizes the critical temperatures $T_{c1}$ and $T_{c2}$ that we have obtained and those obtained in the literature.

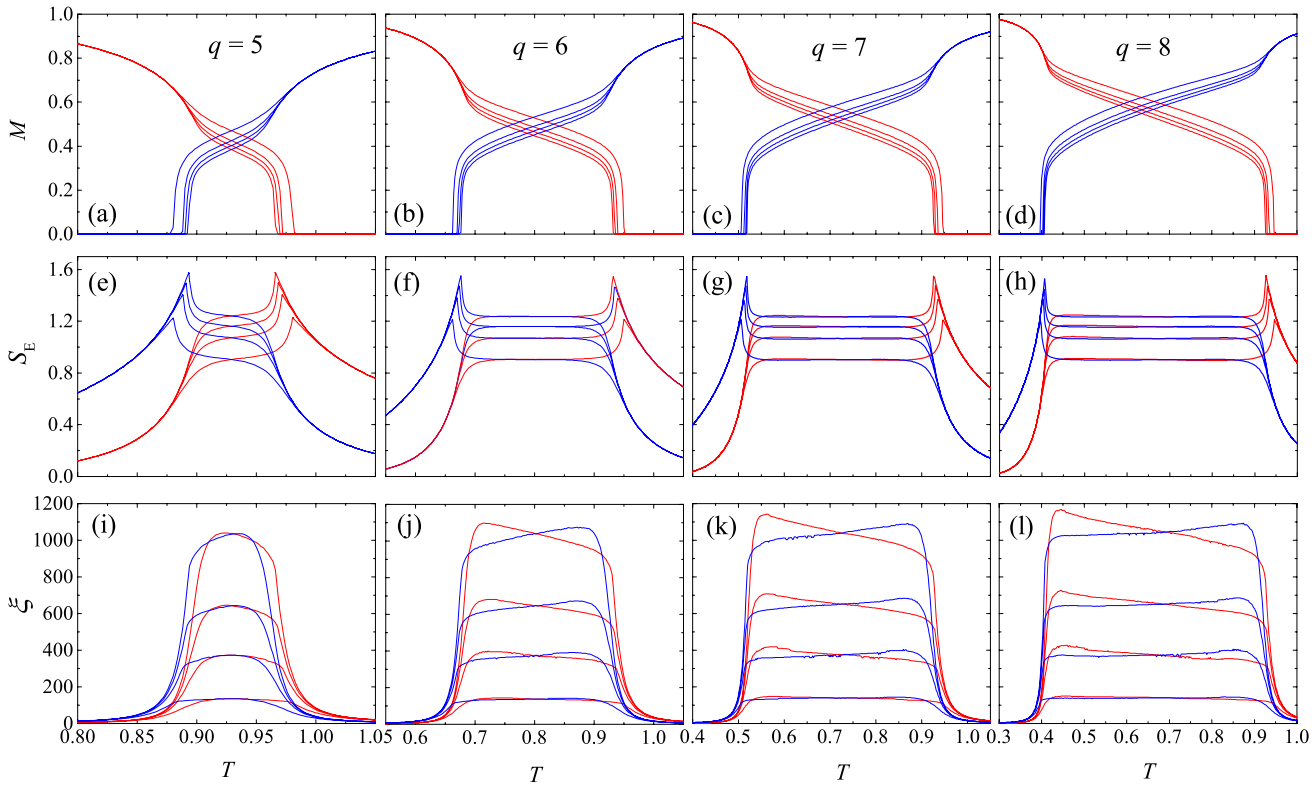


Figure S1. The first row shows the magnetization as a function of temperature $T$ for the clock models (red curves) and their corresponding dual models (blue curves) with $q = 5, 6, 7, 8$, respectively. Similarly, the second and third rows show the entanglement entropy and the correlation length of the clock models and their dual models, respectively. In each figure, the bond dimension for each curve from bottom to top is $D = 50, 110, 170$ and $250$, respectively.

### C. $\mathbb{Z}_q$-deformed sine-Gordon theory

The effective field theory describing the $q$-state clock model is the so-called $\mathbb{Z}_q$-deformed sine-Gordon model, which is defined through its action [S21, S22]

$$S = \frac{1}{2\pi K}\int d^2\mathbf{r}(\nabla\phi)^2 + \frac{g_1}{2\pi\alpha^2}\int d^2\mathbf{r}\cos(\sqrt{2}\phi) + \frac{g_2}{2\pi\alpha^2}\int d^2\mathbf{r}\cos(q\sqrt{2}\Theta), \tag{S22}$$

where the real scalars $\phi$ and $\Theta$, being compactified on a circle as $\phi \equiv \phi + \sqrt{2}\pi$ (same for $\Theta$), are mutually dual to each other, i.e., $\partial_x\phi = -K\partial_y\Theta$ and $\partial_y\phi = K\partial_x\Theta$.

The physics of the $q$-state clock model with $q = 2, 3, 4$ can be easily understood from the above field theory [S23, S24]. For $q = 2$ and 3, either of the two cosine terms is relevant, and the model is thus generically off-critical. However, the self-dual point is very special and remains critical, where the relevant perturbations drive the free-boson CFT (with central charge $c = 1$) to new strong coupling fixed points (with $c < 1$ according to Zamolodchikov's $c$ theorem). For $q = 2$, the cosine terms (having scaling dimension 1) can be refermionized, and the resulting theory at the self-dual point is a free massless Majorana fermion (Ising CFT with $c = 1/2$). For $q = 3$, the self-dual case corresponds to an integrable deformation of the $\mathbb{Z}_4$ parafermion CFT [S23, S25], and the strong coupling fixed point is the $\mathbb{Z}_3$ parafermion CFT (with $c = 4/5$). For $q = 4$, both cosine terms are marginally irrelevant at $K = 4$ (otherwise one of them is relevant). As there is only one critical point (manifestly self-dual via the Kramers-Wannier duality transformation) in the $q = 4$ clock model, we can safely identify this with the field theory (S22) with $K = 4$ and $g_1 = g_2$, which is also self-dual and, in fact, maps to two copies of Ising CFTs. In this way, the correspondence between the self-dual critical point of the $q$-state clock model (S1) for $q = 2, 3, 4$ and the $\mathbb{Z}_q$-deformed sine-Gordon model (S22) with $K_{\rm sd} = q$ and $g_1 = g_2$ is established.

For $q > 4$, we have discussed the predictions of the above $\mathbb{Z}_q$-deformed sine-Gordon model in the main text. Below we only supplement the derivation of the critical exponent $\eta = 1/K$ for the spin-spin correlation function within the BKT critical phase.

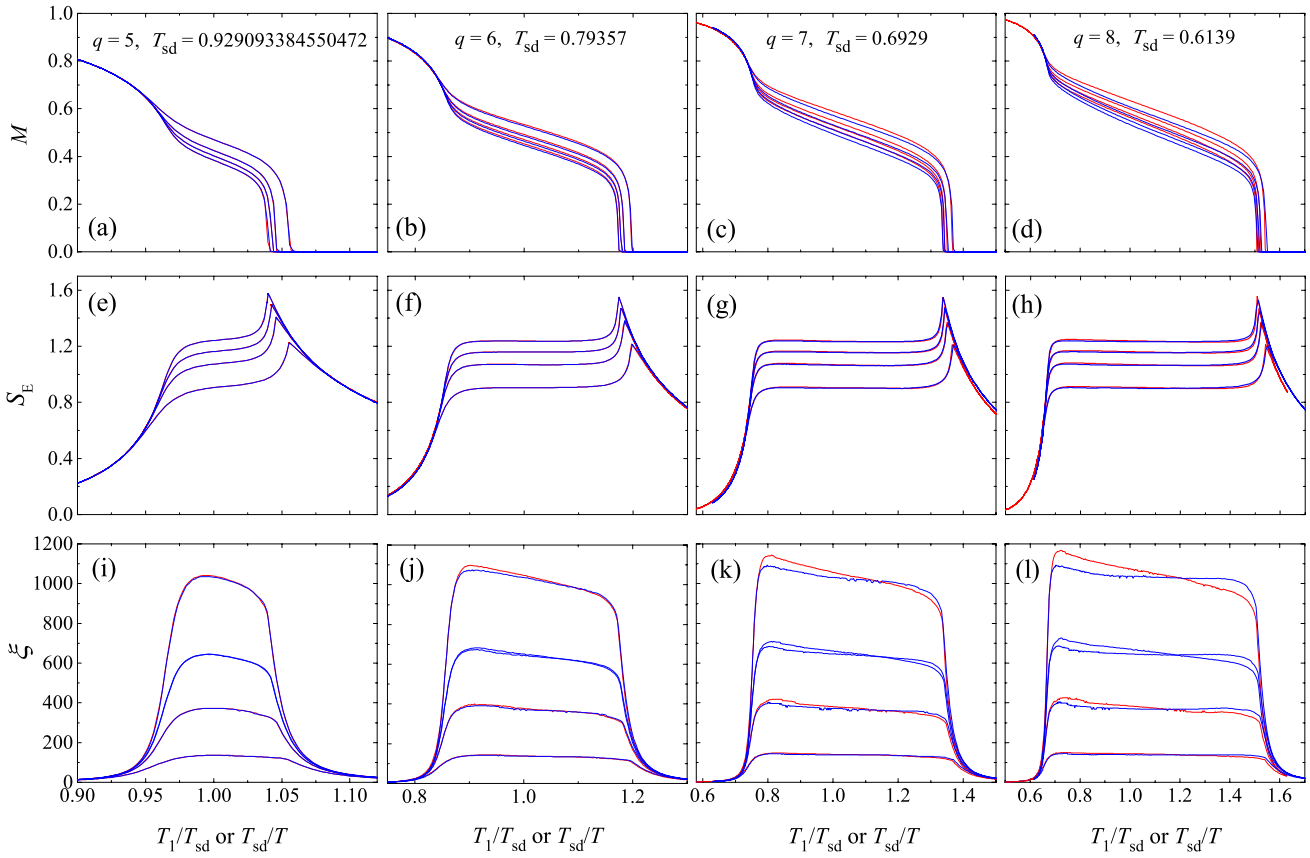


Figure S2. Magnetization $M$ (first row), entanglement entropy $S_E$ (second row) and correlation length $\xi$ (third row) as a function of the rescaled temperature $T/T_{sd}$ for the clock model and the rescaled inverse temperature $T_{sd}/T$ for the dual model. In each figure, the bond dimension for each curve from bottom to top is $D = 50, 110, 170$ and $250$, respectively.

Within the critical phase, the effective action, after dropping the two irrelevant cosine terms, corresponds to a free boson CFT

$$S = \frac{1}{2\pi K} \int d^2\mathbf{r} (\nabla\phi)^2. \tag{S23}$$

For the free boson CFT (S23), the two-point correlation function between $O_{m,n} = \exp(im\sqrt{2}\phi)\exp(in\sqrt{2}\Theta)$ and $O_{-m,-n}$ is given by [S22]

$$\langle O_{m,n}(\mathbf{r_1}) O_{-m,-n}(\mathbf{r_2})\rangle = \exp\left[-2\Delta_{m,n}\log\left(\frac{|\mathbf{r}_{12}|}{\alpha}\right) - 2is_{m,n}\left(\mathrm{Arg}(\mathbf{r}_{12}) + \frac{\pi}{2}\right)\right], \tag{S24}$$

where $\alpha$ is the ultraviolet cutoff, $\mathrm{Arg}(\mathbf{r}_{12})$ is the polar angle of the vector $\mathbf{r}_{12} = \mathbf{r_1} - \mathbf{r_2}$. Here $\Delta_{m,n}$ and $s_{m,n}$ are the scaling dimension and the conformal spin of $O_{m,n}$,

$$\Delta_{m,n}(K) = \frac{1}{2}\left(m^2K + \frac{n^2}{K}\right), \quad s_{m,n} = mn, \tag{S25}$$

respectively.

To establish the correspondence between the above correlation function and the correlation function of the lattice spins, we should first know the correspondence between the scalar fields and the lattice spin variables. From the symmetry analysis of the action (S22), the scalar fields $\phi$ and $\Theta$ should be related to the vortex and lattice (clock) spins, respectively. Meanwhile, it is worth noting that the field $\Theta$ has been compactified with $\Theta \equiv \Theta + \sqrt{2}\pi$, while the periodicity of the lattice spin is $2\pi$. Thus, the clock spin on the lattice, in the continuum limit, can be identified with $O_{0,1} = \exp(i\sqrt{2}\Theta)$ (up to higher order terms with larger scaling dimensions). According to Eq. (S24), the critical exponent $\eta$ of the correlation function between the clock spins is therefore $\eta = 2\Delta_{0,1} = 1/K$.

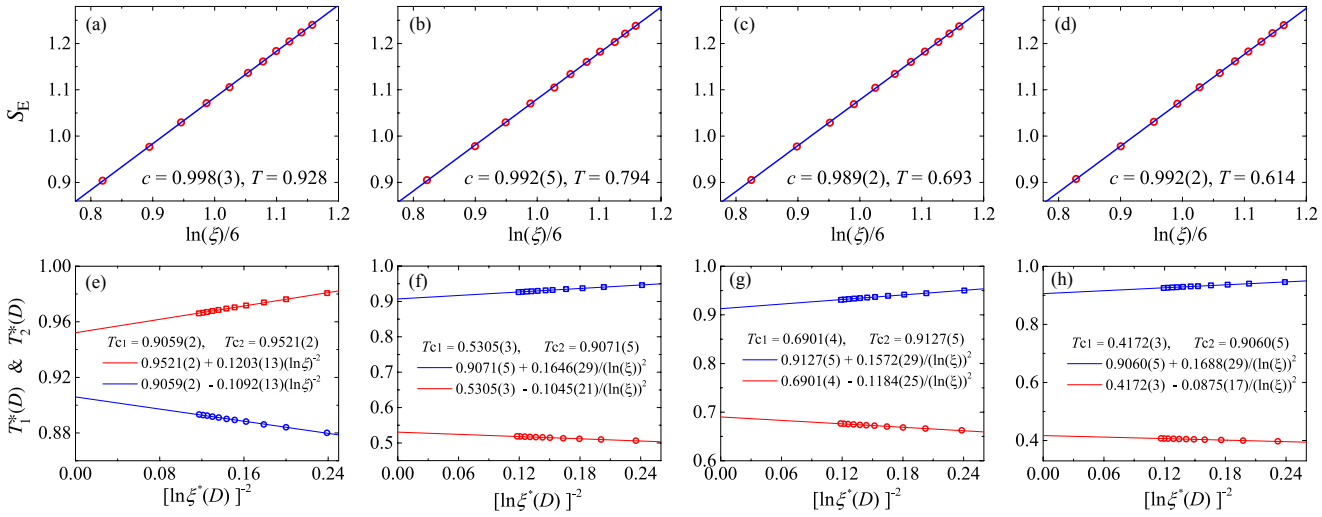


Figure S3. The first row shows the central charge $c$ extracted by linearly fitting the slope between $S_{\rm E}$ and $\ln(\xi)/6$ at representative point $T = 0.928, 0.794, 0.693$ and $0.614$ in the critical phase for $q = 5, 6, 7$ and $8$, respectively. The second row shows the critical temperatures $T_{c1}$ and $T_{c2}$ extracted by linearly extrapolating the peak positions $T_1^*(D)$ and $T_2^*(D)$ of $S_{\rm E}$ with $(\ln\xi^*(D))^{-2}$, where $\xi^*(D)$ is the correlation length at the peak position for a given bond dimension $D$.

### D. Derivation of the boson radius $R = \sqrt{2K}$ for $q \geq 5$

The recently proposed Klein bottle entropy approach [S26–S30] provides a convenient way for determining $K$ [see Eq. (S22)] directly from the microscopic model (S1). It was shown in Ref. [S30] that the Klein bottle entropy is directly related to the boson radius $R$. However, the calculation in Ref. [S30] was done with the convention in Ref. [S31]. Therefore, we have to translate the field theory (S22) into the compactified boson conformal field theory used in Ref. [S31] [see Eq. (6.40) with $g = 1/4\pi$ and Eq. (6.90)].

For this, making use of the dual relation

$$\partial_x\phi = -K\partial_y\Theta, \qquad \partial_y\phi = K\partial_x\Theta, \tag{S26}$$

we can rewrite (S22) as

$$S = \frac{K}{2\pi}\int d^2\mathbf{r}(\nabla\Theta)^2 + \frac{g_1}{2\pi\alpha^2}\int d^2\mathbf{r}\cos(\sqrt{2}\phi) + \frac{g_2}{2\pi\alpha^2}\int d^2\mathbf{r}\cos(q\sqrt{2}\Theta), \tag{S27}$$

where the fields $\phi$ and $\Theta$ are periodic

$$\phi \equiv \phi + \sqrt{2}\pi, \qquad \Theta \equiv \Theta + \sqrt{2}\pi. \tag{S28}$$

Then, we rescale the fields $\phi$ and $\Theta$ in Eq. (S27) as

$$\phi' = \frac{1}{2\sqrt{K}}\phi, \qquad \Theta' = 2\sqrt{K}\Theta, \tag{S29}$$

whose periodicity becomes

$$\phi' \equiv \phi' + 2\pi/\sqrt{2K}, \qquad \Theta' \equiv \Theta' + 2\pi\sqrt{2K}. \tag{S30}$$

After the rescaling, the action in (S27) now takes the form

$$S = \frac{1}{8\pi}\int d^2\mathbf{r}\left(\nabla\Theta'\right)^2 + \frac{g_1}{2\pi\alpha^2}\int d^2\mathbf{r}\cos\left(2\sqrt{2K}\phi'\right) + \frac{g_2}{2\pi\alpha^2}\int d^2\mathbf{r}\cos\left(\frac{q}{\sqrt{2K}}\Theta'\right). \tag{S31}$$

Since both cosine terms are irrelevant for $T_{c1} < T < T_{c2}$, the effective theory is

$$S \simeq \frac{1}{8\pi}\int d^2\mathbf{r}\left(\nabla\Theta'\right)^2, \tag{S32}$$

whose scalar field $\Theta'$ has compactification radius $R = \sqrt{2K}$ [see also Eq. (6.90) in Ref. [S31]].

Table S1. Comparison of the critical temperatures $T_{c1}$ and $T_{c2}$ for the clock model with $q = 5, 6, 7$ and 8.

| $q = 5$ | $T_{c1}$ | $T_{c2}$ |
|---|---|---|
| Ref. [S4](1982) | 0.8 | 1.1 |
| Ref. [S5](2011) | 0.905(1) | 0.951(1) |
| Ref. [S6](2013) | 0.908 | 0.944 |
| Ref. [S7](2014) | 0.914(12) | 0.945(17) |
| Ref. [S8](2018) | 0.897(1) | - |
| Ref. [S9](2018) | 0.9029(1) | 0.9520(1) |
| Ref. [S10](2019) | 0.911(5) | 0.940(5) |
| Ref. [S11](2019) | 0.908 | 0.945 |
| Present work | 0.9059(2) | 0.9521(2) |
| $q = 6$ | $T_{c1}$ | $T_{c2}$ |
| Ref. [S4](1982) | 0.6 | 1.3 |
| Ref. [S12](1986) | 0.68(2) | 0.92(1) |
| Ref. [S13](1991) | 0.68 | 0.90 |
| Ref. [S14](2002) | 0.7014(11) | 0.9008(6) |
| Ref. [S15](2009) | 0.632(2) | 0.997(2) |
| Ref. [S16](2010) | 0.68(1) | 0.90(1) |
| Ref. [S17](2013) | - | 0.9020(5) |
| Ref. [S6](2013) | 0.700(4) | 0.904(5) |
| Ref. [S18](2016) | 0.70 | 0.88 |
| Ref. [S1](2017) | 0.6658(5) | 0.8804(2) |
| Ref. [S8](2018) | 0.681(1) | - |
| Ref. [S10](2019) | 0.701(5) | 0.898(5) |
| Ref. [S11](2019) | 0.693 | 0.904 |
| Present work | 0.6901(4) | 0.9127(5) |
| $q = 7$ | $T_{c1}$ | $T_{c2}$ |
| Ref. [S19](2012) | 0.533 | 0.900 |
| Ref. [S8](2018) | 0.531(6) | - |
| Present work | 0.5305(3) | 0.9071(5) |
| $q = 8$ | $T_{c1}$ | $T_{c2}$ |
| Ref. [S14](2002) | 0.4259(4) | 0.8936(7) |
| Ref. [S20](2009) | 0.417(3) | 0.894(1) |
| Ref. [S8](2018) | 0.418(1) | - |
| Present work | 0.4172(3) | 0.9060(5) |

### E. Klein bottle entropy approach

Here we briefly review how to calculate the Klein bottle ratio [S26–S30]

$$g = \frac{Z^{\mathcal{K}}(2L_x, L_y/2)}{Z^{\mathcal{T}}(L_x, L_y)}, \tag{S33}$$

which directly gives the compactification radius $R = \sqrt{2K}$ for the compactified boson CFT [S30] or is related to the quantum dimensions of the primary fields for the rational CFT [S26].

Fig. S4(a) corresponds to the Klein bottle partition function with length $2L_x$ and width $L_y/2$, which is difficult to calculate directly. It is more convenient to convert it to a cylinder with crosscap boundaries [as shown in Fig. S4(b-d)] by the clip, flip and sew procedures, where the spatial reflection symmetry of the system has been used in the flip procedure. Since Eq. (S33) is valid for $L_x \gg L_y$, the calculation of the Klein bottle partition function can be performed in the limit of $L_x \to \infty$, for which only the leading eigenvector of the column-to-column transfer matrix is needed [see Fig. S4(e)]. In order to obtain this leading eigenvector, we first convert the periodic column-to-column transfer matrix to a transfer matrix with open boundary [see Fig. S4(f)], and then use the DMRG algorithm to obtain its leading eigenvector, which is approximated by a MPS with bond dimension $D$. Once the MPS is obtained, the ratio of the Klein bottle and torus partition functions can be calculated as shown in Fig. S4(h).

Fig. S5 shows the Klein bottle ratio $g$ for the clock models with $q = 2, 3, 4$. It is clearly seen that the curves for different $L_y$ intersect at the self-dual points, where second-order phase transitions occur. For these second-order transition points, the Klein bottle ratios $g$ at the critical points of the $q = 2, 3$ and 4 clock model are related to the quantum dimensions of the primary fields [S26, S27].

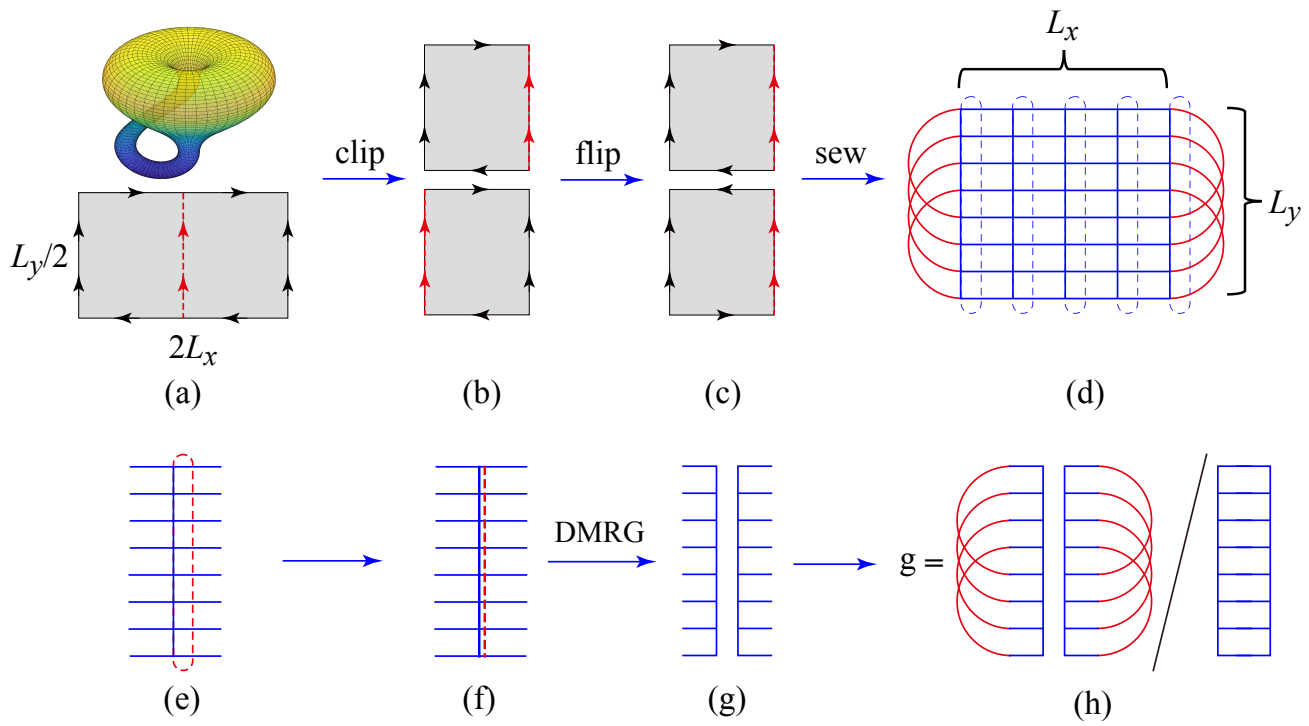


Figure S4. The method for calculating the ratio between the Klein bottle and torus partition functions. The Klein bottle partition function in (a) is converted into a cylinder with crosscap boundaries in (d) via (b) clip and (c) flip-and-sew procedures. The bulk of the cylinder is defined via the column-to-column transfer matrix with (e) periodic and (f) open boundaries, whose leading vector is approximated by an MPS by using the DMRG algorithm in (g). (h) The Klein bottle ratio $g$ is obtained by contracting the MPS under properly defined boundaries.

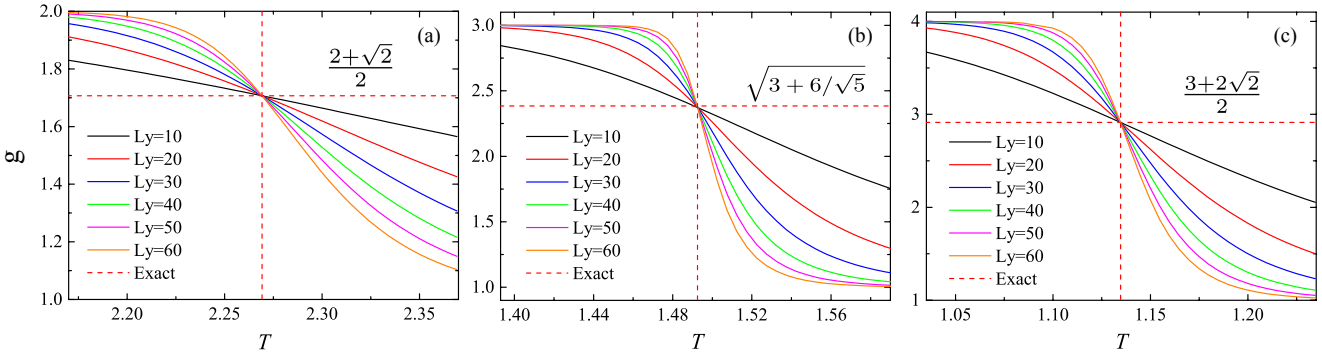


Figure S5. The Klein bottle ratios $g$ as a function of temperature $T$ for (a) the Ising model ($q = 2$), (b) $q = 3$ clock model, and (c) $q = 4$ clock model. The different curves correspond to calculations with different $L_y$. The vertical dashed lines indicate the known second-order transition points. The horizontal lines are the Klein bottle ratios at the critical points, which are predicted by CFTs [S26, S27].

* hong-hao.tu@tu-dresden.de
† navyphysics@iphy.ac.cn
‡ txiang@iphy.ac.cn

[S1] J. Chen, H.-J. Liao, H.-D. Xie, X.-J. Han, R.-Z. Huang, S. Cheng, Z.-C. Wei, Z.-Y. Xie, and T. Xiang, Chin. Phys. Lett. **34**, 050503 (2017).
[S2] H. A. Kramers and G. H. Wannier, Phys. Rev. **60**, 252 (1941).
[S3] V. Zauner-Stauber, L. Vanderstraeten, M. T. Fishman, F. Verstraete, and J. Haegeman, Phys. Rev. B **97**, 045145 (2018).
[S4] J. Tobochnik, Phys. Rev. B **26**, 6201 (1982).
[S5] O. Borisenko, G. Cortese, R. Fiore, M. Gravina, and A. Papa, Phys. Rev. E **83**, 041120 (2011).

[S6] Y. Kumano, K. Hukushima, Y. Tomita, and M. Oshikawa, Phys. Rev. B **88**, 104427 (2013).
[S7] C. Chatelain, J. Stat. Mech. **2014**, 11022 (2014).
[S8] S. Chatterjee, S. Puri, and R. Paul, Phys. Rev. E **98**, 032109 (2018).
[S9] Y. Chen, Z.-Y. Xie, and J.-F. Yu, Chin. Phys. B **27**, 080503 (2018).
[S10] T. Surungan, S. Masuda, Y. Komura, and Y. Okabe, J. Phys. A **52**, 275002 (2019).
[S11] S. Hong and D.-H. Kim, arXiv:1906:09036 (2019).
[S12] M. S. S. Challa and D. P. Landau, Phys. Rev. B **33**, 437 (1986).
[S13] A. Yamagata and I. Ono, J. Phys. A **24**, 265 (1991).
[S14] Y. Tomita and Y. Okabe, Phys. Rev. B **65**, 184405 (2002).
[S15] C.-O. Hwang, Phys. Rev. E **80**, 042103 (2009).
[S16] A. F. Brito, J. A. Redinz, and J. A. Plascak, Phys. Rev. E **81**, 031130 (2010).
[S17] S. K. Baek, H. Mäkelä, P. Minnhagen, and B. J. Kim, Phys. Rev. E **88**, 012125 (2013).
[S18] R. Krčmár, A. Gendiar, and T. Nishino, arXiv:1612.07611 (2016).
[S19] O. Borisenko, V. Chelnokov, G. Cortese, R. Fiore, M. Gravina, and A. Papa, Phys. Rev. E **85**, 021114 (2012).
[S20] S. K. Baek, P. Minnhagen, and B. J. Kim, Phys. Rev. E **80**, 060101 (2009).
[S21] P. B. Wiegmann, J. Phys. C **11**, 1583 (1978).
[S22] H. Matsuo and K. Nomura, J. Phys. A **39**, 2953 (2006).
[S23] P. Lecheminant, A. O. Gogolin, and A. A. Nersesyan, Nucl. Phys. B **639**, 502 (2002).
[S24] W. Li, S. Yang, H.-H. Tu, and M. Cheng, Phys. Rev. B **91**, 115133 (2015).
[S25] V. Fateev and A. Zamolodchikov, Phys. Lett. B **271**, 91 (1991).
[S26] H.-H. Tu, Phys. Rev. Lett. **119**, 261603 (2017).
[S27] W. Tang, L. Chen, W. Li, X. C. Xie, H.-H. Tu, and L. Wang, Phys. Rev. B **96**, 115136 (2017).
[S28] L. Chen, H.-X. Wang, L. Wang, and W. Li, Phys. Rev. B **96**, 174429 (2017).
[S29] H.-X. Wang, L. Chen, H. Lin, and W. Li, Phys. Rev. B **97**, 220407 (2018).
[S30] W. Tang, X. C. Xie, L. Wang, and H.-H. Tu, Phys. Rev. B **99**, 115105 (2019).
[S31] P. D. Francesco, P. Mathieu, and D. Sénéchal, *Conformal Field Theory* (Springer-Verlag, New York, 1997).